Nitrogen Doped Graphene Supported Mixed Metal Sulfide Photocatalyst for High Production of Hydrogen Using Natural Solar Light

Daniel Arulraj Abraham, Aswathy Rajan, M.D Dhileepan, Masakazu Anpo, Bernaurdshaw Neppolian

PII: S0920-5861(22)00471-0

DOI: https://doi.org/10.1016/j.cattod.2022.12.002

Reference: CATTOD13971

To appear in: *Catalysis Today*

Received date: 23 September 2022
Revised date: 24 November 2022
Accepted date: 7 December 2022

Please cite this article as: Daniel Arulraj Abraham, Aswathy Rajan, M.D Dhileepan, Masakazu Anpo and Bernaurdshaw Neppolian, Nitrogen Doped Graphene Supported Mixed Metal Sulfide Photocatalyst for High Production of Hydrogen Using Natural Solar Light, *Catalysis Today,* (2022) doi:https://doi.org/10.1016/j.cattod.2022.12.002

Nitrogen Doped Graphene Supported Mixed Metal Sulfide Photocatalyst for High Production of Hydrogen Using Natural Solar Light

Daniel Arulraj Abraham[a], Aswathy Rajan[b], M.D. Dhileepan[c], Masakazu Anpo[d,e], Bernaurdshaw Neppolian[b]*

[a] School of Engineering, Cardiff University, Cardiff, United Kingdom.

[b]Department of Chemistry, SRM Institute of Science and Technology, Kattankulathur, Chennai, 603203, India

[c]Department of Physics and Nanotechnology, SRM Institute of Science and Technology, Kattankulathur, Chennai, 603203, India

[d]Department of Applied Chemistry Graduate School of Engineering, Osaka Prefecture University (now, Osaka Metropolitan University), Sakai, Osaka 599-8531, Japan

[e]State Key Laboratory of Photocatalysis on Energy and Environment, Fuzhou University, Fuzhou, Fujian 350116, P. R. China

*Corresponding authors -neppolib@srmist.edu.in

Abstract

We have developed a strategy to prevent the photo-corrosion of cadmium sulfide nanorods (CdSNRs) by coating them with cerium sulfide (Ce_2S_3) as co-catalyst and N-doped Graphene (NG) for a solar light-driven H_2 production application. The uniform deposition and coating of Ce_2S_3 and NG over the CdSNRs were confirmed by both FESEM and HRTEM analyses. The incorporation of Ce_2S_3 and NG into CdSNRs not only increased its stability but also extended its absorption in visible and NIR regions. As a result, the prepared CdSNRs/Ce_2S_3 photocatalysts produced ~16,181 μmol h^{-1} g^{-1} of H_2 under solar light irradiation, which was ~ 10 times higher than the pure CdSNRs. Interestingly, N atom doped graphene-supported CdSNRs/Ce_2S_3 photocatalysts has shown a paramount effect on the H_2 production by 24 times higher compared to bare CdSNRs (35,946 μmol $h^{-1}g^{-1}$). In addition, the NG-CdSNRs/Ce_2S_3 photocatalysts

exhibited high stability up to 5 continuous cycles. The high stability was achieved due to the covering of CdSNRs by Ce_2S_3 and NG, which may effectively prevent the leaching out of S^{2-} ions from CdSNRs. On the other hand, the NG played a dual role by preventing the photo-corrosion and also improving the charge carrier separation as evidenced by the PL, TRPL, and Impedance studies. The present work may open a new direction in designing a highly photostable metal sulfide photocatalyst for energy conversion applications in aqueous medium.

Keywords: Photocatalyst, CdS-Ce_2S_3, N doped Graphene, Hydrogen production, Solar light

1. Introduction

Currently, 95% of the industrial scale H_2 is produced from fossil fuels, and most of it is via the steam methane reforming (SMR) method. However, SMR is a complex and costly method and it produces carbon dioxide as a by-product along with H_2. On the other hand, H_2 production via solar water splitting (SWS) and biomass reforming is considered a clean, sustainable, and environmentally friendly energy carrier to replace fossil fuels[1,2]. The SWS method is simple in design, cost-effective, and produces no CO_2 emissions. Water and sunlight are copious and renewable resources on earth and hence, the photocatalytic splitting of water is one of the most promising methods to produce H_2 [3]. Semiconducting photocatalysts are low-cost and provide adjustable energy band gap for solar light absorption [4].

Since Honda and Fujishima discovered the sensitizing effect of TiO_2 semiconductor electrode in the electrochemical photolysis of water with Pt counter electrode in 1972 [5], several semiconductors such as TiO_2, ZnO, and CdS have been applied to study the photocatalytic splitting of water to produce H_2 [6]. Most of the well-known photocatalysts are wide band gap

semiconductors and can only be excited by UV light irradiation, which accounts for only ~4 % of solar energy [7, 8]. Therefore, narrow band gap visible light active photocatalysts are essential to utilize photons energy in the visible region, which is ~46% of solar energy reaching on earth's surface. Modak et al [9] reported photocatalytic H_2 production from water by using Pt-loaded 9,9'-spirobifluorene based-conjugated microporous polymer (Pt/COP-3). Here H_2 was produced by the photocatalyst under visible light irradiation in the presence of triethanolamine (TEOA) as a sacrificial agent. Transition metal dichalcogenides such as metal sulfides and metal selenides are widely used in several applications like catalysts, H_2 production, energy storage, etc. Singh et al [10] suggested MoS_2 has been used as a photocatalyst for H_2 production and CO_2 photoreduction.

Among the numerous visible light active photocatalysts, Cadmium sulfide (CdS) is considered an excellent visible light active semiconducting photocatalyst for solar energy conversion applications due to its appropriate redox potentials and visible light active energy band gap (2.4 eV). CdS produce H_2 because its conduction band edge potential is more negative than the water reduction potential w.r.t. Normalized hydrogen electrode (NHE) [11]. However, it suffers from photo-corrosion and shows instability during the catalytic reaction because of S^{2-} oxidation by photogenerated holes and leaching out of Cd^{2+} ion [12]. Several strategies such as removing the oxygen from the photocatalytic system, use of perfluorodecalin, and anti-photo corrosion layer (Al_2O_3, Cr_2O_3, etc.) have been adopted in the past to overcome these challenges with partial success [13].

Herein, we have used a novel strategy to inhibit S^{2-} oxidation and Cd^{2+} leaching by incorporating N-doped Graphene (NG) as supporting material and Ce_2S_3 as the co-catalyst. CdSNRs covered by NG and Ce_2S_3 nanoparticles have also been applied to realize a high photoelectrochemical performance from ultraviolet to NIR with photocurrent enhancement. The NG provides a large surface area, excellent conductivity, high catalytic sites, and tunable electronic properties [14]. Previous studies such as by Li et al have also reported that NG/CdS can retard the recombination of photoelectron-hole pair and improves photocatalytic H_2 production [15]. However, there has been no report on Ce_2S_3 works as a co-catalyst and extends the absorption to NIR light. which correlated to enhancing the photocatalytic performance of CdS-based nanostructure, particularly for H_2 production. In this study, a photocatalyst consisting of nanoscale NG-CdSNRs/Ce_2S_3 heterostructures were successfully fabricated and characterized by various techniques. The structural and optical properties of photocatalysts were characterized by FESEM, HRTEM, and UV-visible-NIR spectrophotometry. The chemical composition and oxidation state of the photocatalysts were studied in detail. The photophysical properties were further determined by photoelectrochemical measurements, and the light-harvesting properties were correlated with the observed photocatalytic performance, which indicates that Ce_2S_3 is an efficient cocatalyst for H_2 production in water under solar light irradiation.

2. Experimental section

2.1. Materials

All chemicals and reagents were of analytical grade and used without further purification. Cadmium chloride monohydrate, cerium III nitrate hexahydrate, ethylenediamine ($H_2NCH_2CH_2NH_2$, 99.0%), thiourea (CH_4N_2S, 99.0%), sodium sulfite (Na_2SO_3) anhydrous were

purchased from Sigma Aldrich. Citric acid, ethanol, and sodium sulfide nonahydrate flakes ($Na_2S.\ 9H_2O$, ≥98.0%) were obtained from Rankem, India. Graphite powder (purity 99.9995%) and urea were purchased from Alpha Aesar.

2.2. Synthesis of CdSNRs

CdS nanorods (CdSNRs) were synthesized by using a simple solvothermal method. Briefly, the cadmium chloride monohydrate was dissolved into 60 mL of ethylenediamine solution. Then, thiourea was added to the above solution and stirred for 5 min. The reaction mixture was transferred into a Teflon-lined autoclave, sealed, and maintained at 160 ^{o}C for 48 h in a muffle furnace. After it is allowed to cool at room temperature, the obtained yellow product was washed with distilled water and ethanol several times. Then, the catalyst was dried at 70 ^{0}C overnight in an oven.

2.3. Synthesis of CdSNRs/Ce_2S_3nanocomposite

For the synthesis of CdSNRs/0.1MCe_2S_3 photocatalyst, 50 mg of CdSNRs and 20 mg of citric acid were initially dissolved in 25 mL distilled water followed by sonication for 15 min. The resulting solution was maintained at 45 ^{0}C for 2h with constant stirring. The cerium III nitrate (0.1M) and Na_2S (0.1M) were added to the reaction solution and again stirred for 1h. Finally, the CdSNRs/0.1MCe_2S_3 catalyst was washed with distilled water and ethanol several times. The obtained CdSNRs/0.1MCe_2S_3 catalyst was then dried at 70 ^{0}C overnight. Similarly, the CdSNRs/0.5MCe_2S_3, CdSNRs/1.0MCe_2S_3, CdSNRs/1.25MCe_2S_3 and Ce_2S_3 (without CdS) photocatalysts were synthesized for H_2 production.

2.4. Synthesis of NG-CdS/Ce_2S_3 photocatalysts

The graphene oxide was prepared from graphite powder (99%) according to the modified Hummers' method. N-doped graphene was prepared by the hydrothermal method. In this process, 120 mg of graphene oxide was dispersed in 70 ml distilled water and then 500 mg of urea was added to the dispersed solution followed by sonication for 2 h. The final solution was kept in a 100 ml Teflon-lined autoclave, heated, and maintained at 180 ^{0}C for 12 h. The obtained NG was collected and then, washed with distilled water/ethanol several times, and dried at 70 °C under in the oven. The synthesis of NG-CdSNRs/Ce_2S_3, different weight ratios (1%, 2%, 3%,4%) of N-doped graphene, 50 mg of CdSNRs, and 20 mg of citric acid were dissolved in 25 ml distilled water followed by sonication for 15 min. The resulting solution was maintained at 45 ^{0}C for 2 h with constant stirring. The cerium (III) nitrate solution (0.5M) and Na_2S solution (0.5M) were added to the reaction solution and stirred for 1h. Finally, the NG-CdSNRs/0.5MCe_2S_3 catalyst was washed with distilled water and ethanol several times. The obtained CdSNRs/0.5MCe_2S_3 catalyst was then dried at 70 ^{0}C overnight.

2.5. Characterisation Studies

Morphology of CdSNRs, CdSNRs/Ce_2S_3, and NG-CdSNRs/Ce_2S_3 photocatalysts was observed with a Field-emission scanning electron microscope (FEI Quanta FEG 200 HR-SEM) and HRTEM (Philips Tecnai 20U-Twin microscope at an acceleration voltage of 200 kV used for capture for HRTEM images). UV-vis diffuse reflection spectroscopy (DRS) was performed by Shimadzu UV-2600 UV-Vis spectrometer.XRD patterns were recorded by X-ray diffractometer (PANalytical X'pert powder diffractometer) using Cu Kα radiation. The chemical states of the catalysts were obtained from X-ray photoelectron spectroscopy (XPS). Which was performed by using a PHI Quantera II XPS spectrometer equipped with a monochromatic Al Kα

X-ray source (hν = 1486.6 eV) Photoelectrochemical studies were carried out by using a Biologic electrochemical workstation (SP-150). A 300WSS–EM Solar simulator was used as the light source for photocurrent measurements. The time-resolved photoluminescence (TRPL) spectra were performed HORIBA FLUORO LOG@3. Electrochemical impedance spectral analysis was carried out by using a Biologic electrochemical work station (SP-150) in 5mM $K_4[Fe(CN)_6]^{3+}$ 0.1M KCl solution at open-circuit voltage over a frequency range from 10^5 to 10^{-1} Hz with an AC voltage at 10 mV. The Mott–Schottky plots were carried out by the CH instrument electrochemical analyzer at a constant frequency (1Hz).

2.6. Photocatalytic activity measurement of NG-CdSNRs/Ce_2S_3

The photocatalytic activity of the NG-CdSNRs/Ce_2S_3 was evaluated by measuring H_2 production under natural solar light. The photocatalyst was dispersed in 50 ml of the sacrificial agent (Na_2S/Na_2SO_3aqueous solution). Initially, nitrogen gas was purged through the glass reactor cell for 30 min to remove air under dark conditions. The H_2 production was monitored by Shimadzu GC-2014 gas chromatography and nitrogen gas was used as carrier gas. Solar to hydrogen (STH) conversion efficiency is one of the main factors to estimate the efficiency in water splitting given as follows,

$$\mathrm{STH} = \frac{\text{Output energy of hydrogen}}{\text{Incident solar light energy}}$$

3. Results and Discussion

3.1.Surface Morphological Studies

The morphology of synthesized CdSNRs, CdSNRs/Ce_2S_3, and NG-CdSNRs/Ce_2S_3 catalysts was observed by FESEM and HRTEM (Fig. 1). FESEM and TEM images of CdS (Fig. 1a and 1c) display nanorods shape (1D) with an average diameter of ~50 nm and length of 0.5-1.2 μm. Fig 1b, 1f, and 1h show the uniform doping of CdS photocatalyst over the support. These images also represented the uniform deposition and coating of Ce_2S_3 and NG over the surface of CdSNRs (Fig1b, 1f, 1g). The Ce_2S_3 co-catalyst formed as nanoparticles (Fig. 1d, 1e) with an average size of 3 nm. Figures 1f, 1g, and 1h show that the Ce_2S_3 nanoparticles [16] are encapsulated onto the nanorods of NG-CdSNRs/Ce_2S_3 heterostructure and clouds of nanoparticles are occupying the nanorods. It may have occurred due to the strain effect of two different sizes of metals and the ligand effect arises between the surface of CdSNRs and the Ce_2S_3 cocatalyst. A similar observation was reported by Nakibli et al [17] with cadmium selenide (CdSe) quantum dot embedded with CdSNRs [17]. HRTEM images shown in Fig. 1i present the resolved lattice fringes of CdSNRs with a lattice spacing of 0.35 nm, which is consistent with the d-spacing value for (002) plane of hexagonal CdSNRs [18]. The lattice fringes of Ce_2S_3 with a spacing of 0.32 nm (031 planes) [16] are shown in Fig. 1j.

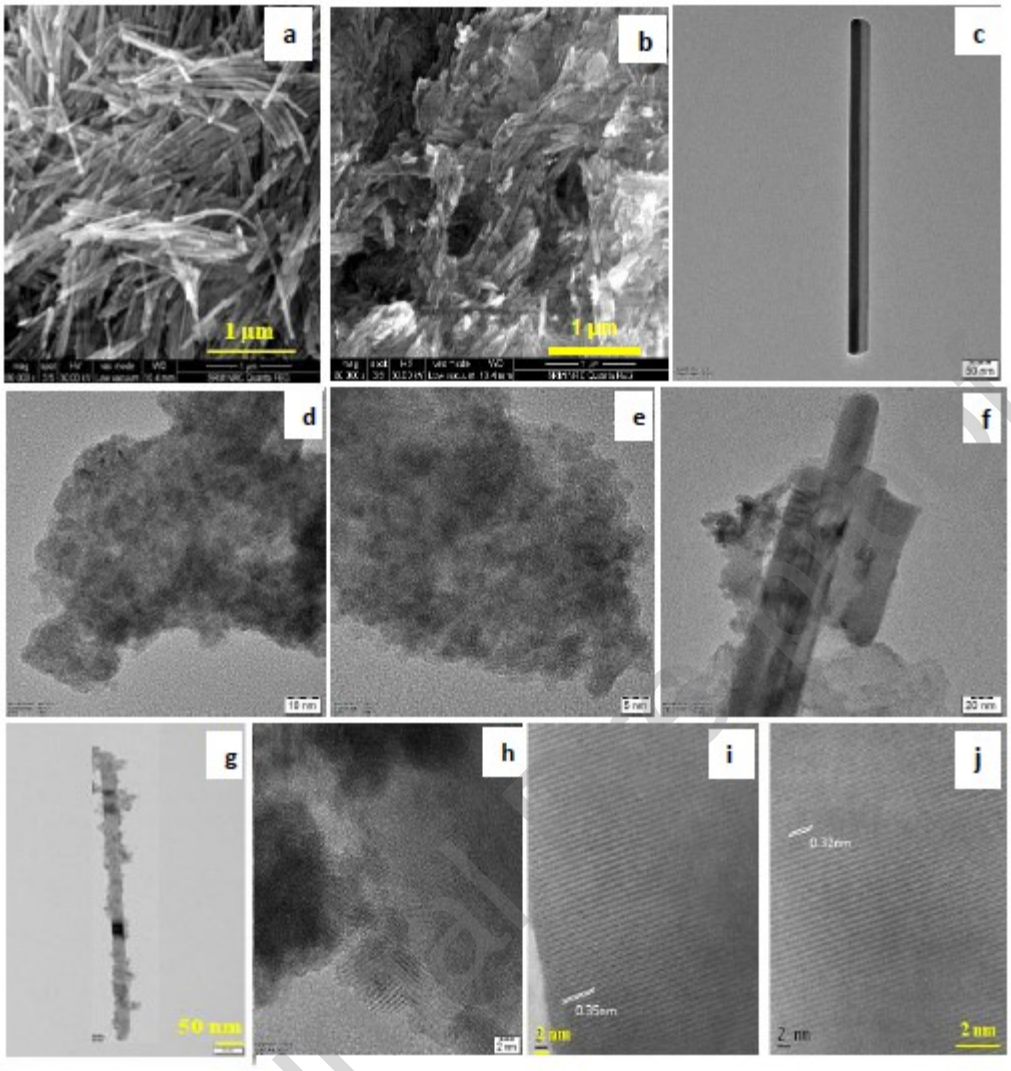

Figure 1. The FESEM & TEM images of CdSNRs (a, c) and FESEM images of 3%NG-CdSNRs/Ce_2S_3 sample (b). TEM image of Ce_2S_3 nanoparticles (d, e), and 3% NG-CdSNRs/Ce_2S_3 sample (f, g); HRTEM images of 3%NG-CdSNRs/Ce_2S_3 sample (h, I, j).

3.2. Structural analysis

XRD patterns of pure CdSNRs, Ce_2S_3, CdSNRs/Ce_2S_3, and NG-CdSNRs/Ce_2S_3 catalysts are shown in Fig. 2. The XRD pattern of the pure CdSNRs shows a highly crystalline hexagonal phase (JCPDS card no. 41-1049) [19] with lattice constants of a = 4.140 Å and c = 6.719 Å. It

can be seen that after the incorporation of 0.25M Ce_2S_3 in CdSNRs, the XRD peak intensity of CdSNRs substantially reduced and further increased the Ce_2S_3 content to 0.5M, and most of the peaks of CdSNRs disappeared. This suggests that Ce_2S_3 covered the CdSNRs surface. Moreover, with the presence of NG in the composites, the diffraction peak intensity of CdSNRs further reduces (Fig. S1) [20]. From the results (Fig 1, 2), it is considered that CdSNRs are encapsulated by Ce_2S_3 and NG, successfully preventing photo corrosion.

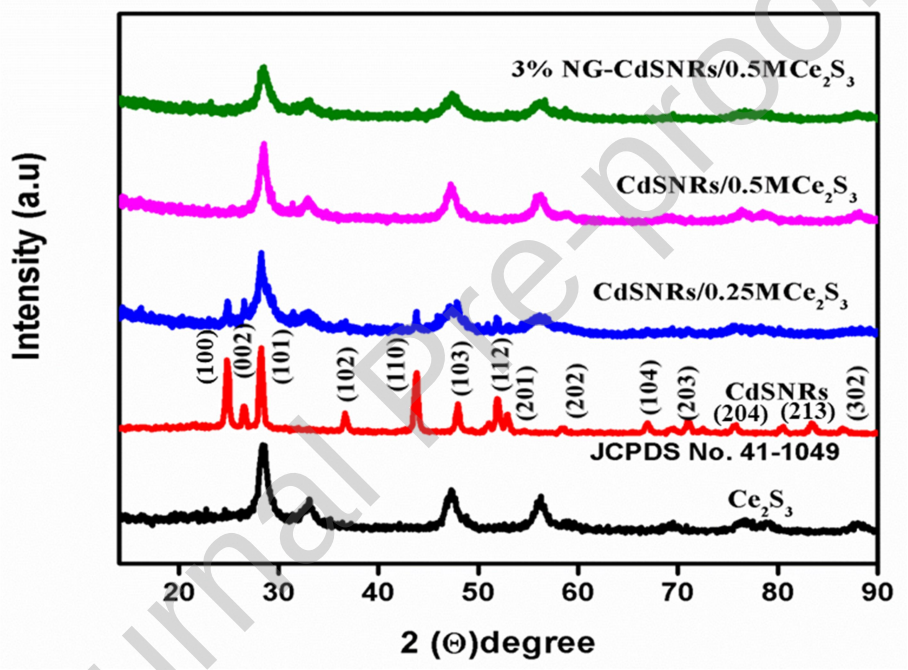

Figure 2. XRD patterns of the CdSNRs, CdSNRs/Ce_2S_3 and 3%NG-CdSNRs/Ce_2S_3 samples

3.3. XPS analysis

Figure 3 (g) shows that the XPS survey scan of the synthesized NG-CdSNRs/Ce_2S_3 catalyst and the presence of Cd (3d), S (2p), Ce (3d, 4d), N1s, and C (1s) elements in the photocatalysts. The binding energy of C1s peaks in Fig. 3 (a, b) at 284.6, 285.8, 286.4, 287.1, 288.5 and 289.1 eV correspond to the sp^2-hybridized carbon (C−C), C-OH, epoxy/ hydroxyl carbon (C−O), carbonyl (C=O), C=C and carboxyl (COOH) functional groups, respectively [21].

Compared to CdSNRs/Ce_2S_3, the XPS peak intensities of C-OH (285.8 eV), C-O (286.4 eV), and COOH (290.0 eV) were found to be slightly reduced, and the peak intensity of C=C enhanced in XPS spectra of NG-CdSNRs/Ce_2S_3. An additional peak at 286.6 eV corresponds to the C−N bond due to the incorporation of NG with CdSNRs/Ce_2S_3. Fig. 3 (e) shows the XPS spectra of N 1s in the as-synthesized NG-CdSNRs/Ce_2S_3. The five types of nitrogen can be indicated in the deconvoluted high-resolution N1s spectra consisting of aromatic N-imines (397.7 eV), pyrrolic-N (398.9 eV), pyridinic-N (400.1 eV), quaternary N (401.3 eV) and oxidized nitrogen (403.1 eV) [22,23]. Similarly, the surface coverage of NG-CdSNRs/Ce_2S_3 displays 17% of aromatic N-imines, 41% of pyrrolic-N, 20 % of pyridinic-N, 12% of quaternary N, and 10 % of oxidized nitrogen.

As shown in Fig. 3 (c), the characteristic peaks of Cd $3d_{5/2}$ and Cd $3d_{3/2}$ at 405.04 and 411.76 eV indicates that cadmium is present in the Cd^{2+} state [24]. The S $2p_{3/2}$ and S $2p_{1/2}$ peaks of the CdSNRs were observed at 161.0 and 162.9 eV (Fig. 3d), respectively. Therefore, revealing that sulfide is present in the CdSNRs instead of the sulfur element [25]. Figure 3(f) shows the Ce^{4+} binding energy states of $3d_{5/2}$ & $3d_{3/2}$ at 898.7, 916.9, and Ce^{3+} states of $3d_{5/2}$ & $3d_{3/2}$ at 884.7 eV and 906.2 eV, respectively for CdSNRs/Ce_2S_3 photocatalysts. Compared to CdSNRs/Ce_2S_3, the XPS spectra of Ce 3d in NG-CdSNRs/Ce_2S_3 show peaks shift with the $3d_{5/2}$ and $3d_{3/2}$ peaks appearing at 898.0 eV and 916.5 eV for Ce^{4+} state, respectively [25,26], and for Ce^{3+}state at 884.0 eV, 905.6 eV, respectively. The lower binding energy shift of Ce 3d peaks occurs because of the presence of a lower electronegative nitrogen atom in NG-CdSNRs/Ce_2S_3, which enhances the electron cloud around the Ce cation [27,28]. The concentration % of Ce^{3+} was measured by using the integrated peak area of Ce^{3+} and the total peak area of Ce 3d spectral data. From the measurement (Fig. S2), the Ce^{3+} concentration in the CdSNRs/Ce_2S_3 and NG-CdSNRs/Ce_2S_3 are

~ 10.20 % and 20.13 % respectively. % Of Ce^{3+} is higher in NG-CdSNRs/Ce_2S_3 than CdSNRs/Ce_2S_3, which represents the higher the oxygen vacancies in NG-CdSNRs/Ce_2S_3. Therefore, it delivers higher catalytic activity. The high % of Ce^{3+} may arise from the charge transfer between the NG and CdSNRs.

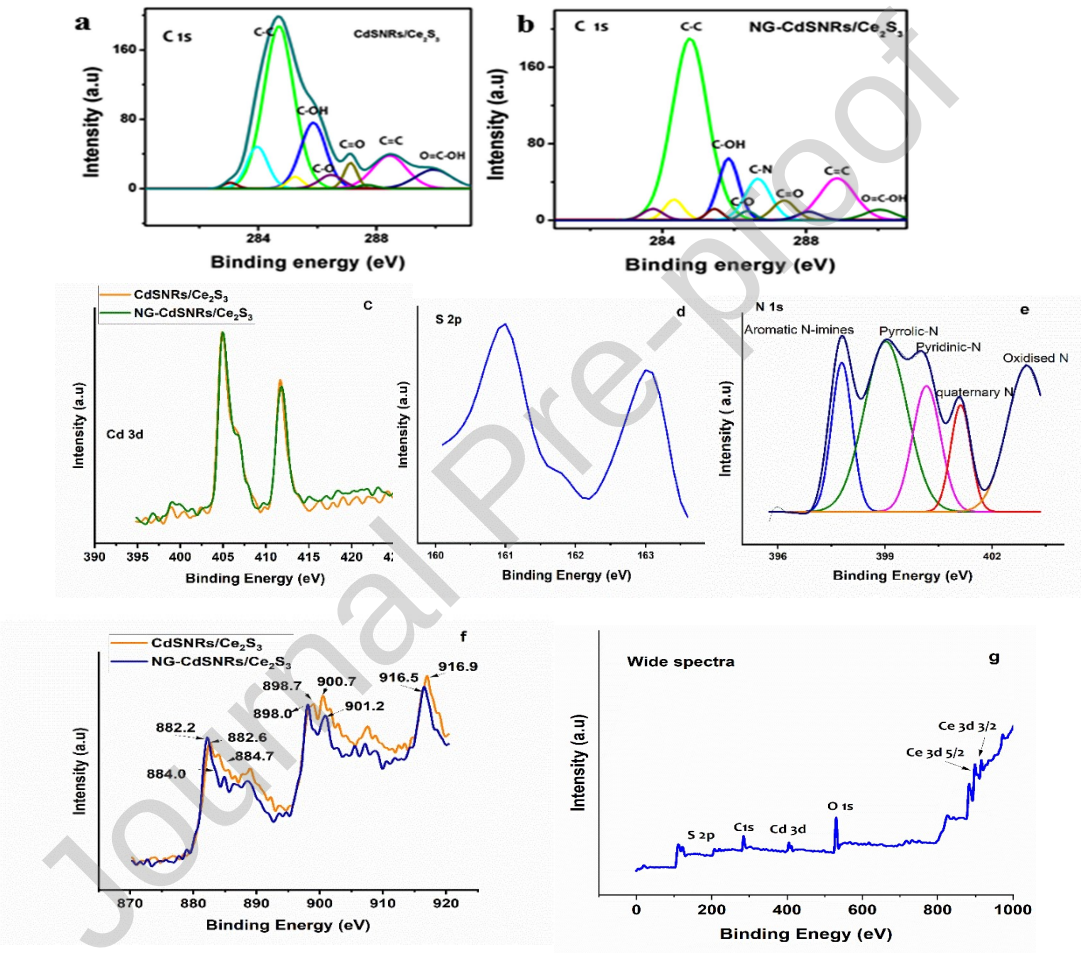

Figure 3. The C1s XPS spectra of (a) CdSNRs/Ce_2S_3, (b) 3% NG-CdSNRs/Ce_2S_3 samples; (c) Cd 3d spectra of CdSNRs/Ce_2S_3 and 3% NG-CdSNRs/Ce_2S_3; (d) S 2p spectrum, (e) N1s spectrum, (f) Ce^{+} spectra, and (g) the survey spectrum of the 3% NG-CdSNRs/Ce_2S_3 samples, respectively.

3.4. Optical characterization

The UV-vis absorbance spectrum of the CdSNRs and CdSNRs/Ce_2S_3 (0.25M, 0.50M,0.75M, 1.00M) and (1%, 2%, 3%, 4 %) of NG-CdSNRs/Ce_2S_3 photocatalysts is shown in Figs. S3 and S4. The CdSNRs showed a band gap of 2.35 eV, which is following the reported value of CdS [29,30]. The visible light absorption (550-900nm) of pure CdSNRs gradually increased with increasing the amount of Ce_2S_3 to 0.5M on the CdSNRs after which it decreased. One important observation is that after Ce_2S_3 coating on the CdSNRs surface, the absorption of CdSNRs/Ce_2S_3 catalyst increased both in the UV and visible regions and the color of the catalyst turned to greenish-yellow from yellow for CdSNRs [31,32]. The absorption edge of NGCdSNRs/Ce_2S_3 photocatalyst was at ~573 nm with a band gap energy of 2.25 eV (Fig. 4B). This is slightly red-shifted from the band edge of pure Ce_2S_3 as shown in Fig. 4A, suggesting that the coupling of CdSNRs with Ce_2S_3 nanoparticles can increase the light absorption capacity of pure Ce_2S_3 and enhance the absorption of visible light. Similarly, the incorporation of NG with the photocatalyst shifted the band edge, it is clear evidence that NG not only is solid support but also interacts with metal, which increases the charge carrier separation and transfer. NG-modified CdSNRs/Ce_2S_3 photocatalyst has wide light absorption from UV to visible light, which is crucial for photocatalytic activity. The absorption enhancement of the NG-CdSNRs/Ce_2S_3 photocatalyst in the visible region can be considered as the synergistic effect of the NG and CdSNRs/Ce_2S_3. This result is consistent with the XPS spectra and can be described in terms of the hybridization of CdSNRs/Ce_2S_3 with NG [33,34].

The charge separation efficiency of the synthesized photocatalysts was evaluated by photoluminescence (PL) spectra at an excitation wavelength of 380 nm, as presented in Fig. S5. After the introduction of Ce_2S_3, the PL intensity of CdSNRs/Ce_2S_3 is remarkably lower than that

of CdSNRs due to the charge carrier transformation between CdSNRs and Ce_2S_3. When the dispersion of NG on the surface of the photocatalyst, the PL intensity significantly decreased. The peak intensity of NG-CdSNRs/Ce_2S_3 was lower than that of the CdSNRs/Ce_2S_3 and pure CdSNRs due to the synergistic effect of the NG and CdSNRs/Ce_2S_3. This confirmed that the photogenerated charge separation efficiency of NG-CdSNRs/Ce_2S_3 was better than the CdSNRs/Ce_2S_3 and CdSNRs. PL results also indicate that the while using NG could prevent the electron-hole pair recombination during the catalytic reaction. Furthermore, TRPL measurements were carried out and the decay spectra indicate the relocation of photogenerated charge carriers of the synthesized photocatalysts (Fig. S6). NG-CdSNRs/Ce_2S_3 and CdSNRs/Ce_2S_3 catalysts showed a longer lifetime of 0.139 ns and 0.132 ns compared with that of 0.126 ns for CdSNRs (Fig. S6). These results confirmed that the electron-hole pair effectively separated in the NG composites compared with pure CdSNRs and CdSNRs/Ce_2S_3 because of the synergistic effect of the NG and CdSNRs/Ce_2S_3. Due to the presence of NG, the efficient charge transfer and separation process occurs at the NG composite, which led to improved photocatalytic H_2 production compared with CdSNRs.

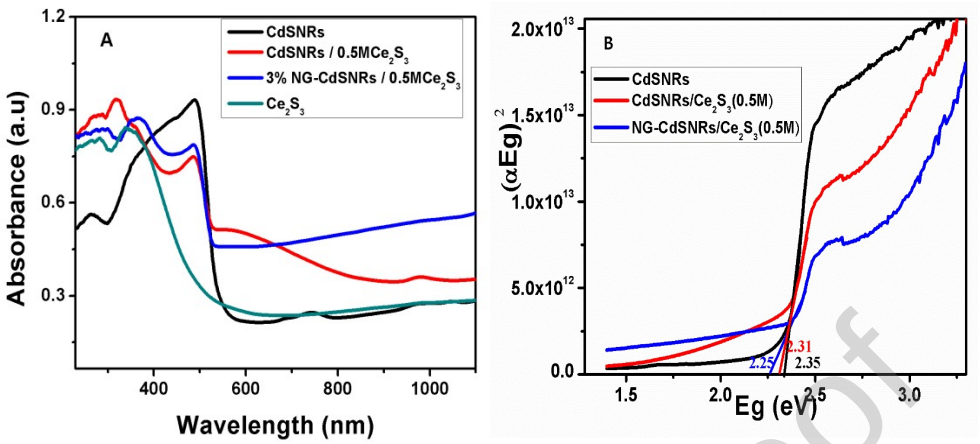

Figure 4. (**A)** Comparison of UV-Vis absorbance spectra of CdSNRs, CdSNRs/ Ce_2S_3, 3% NG-CdSNRs/ Ce_2S_3 and Ce_2S_3 nanocatalysts. (**B)** Plots of the $(aEg)^2$ vs. Eg (eV) for synthesized photocatalyst

3.5. Electrochemical performance

The charge transfer process of the photocatalysts was further studied by the electrochemical impedance spectral analysis (EIS) method (Fig. 5 a). Generally, the diameter of the semicircle is equal to the charge transfer resistance (Rct) of the photocatalysts [35, 36], and Rct values of pure CdSNRs, CdSNRs/Ce_2S_3, NG-CdSNRs/Ce_2S_3 were 357, 220 and 182 Ω, respectively. The results show that the charge transfer resistance of the NG-CdSNRs/Ce_2S_3 is less than the pure CdSNRs and CdSNRs/Ce_2S_3 (0.5M), owing to the presence of N atom doped graphene in the nanocomposite, demonstrating its superior electronic conductivity [37]. The NG in NG-CdSNRs/Ce_2S_3 acts as an effective electron collector and prevents charge recombination. Therefore, these photocatalysts effectively may be expected to produce a huge amount of H_2.

Additionally, the capacitance of modified electrodes [CdSNRs, CdSNRs/Ce_2S_3, NG-CdSNRs/Ce_2S_3] was measured in the three-electrode cell (potential range from 0.2 V to -0.85 V) by Mott-Schottky experiments. Based on these capacitance results, the flat band potential of the modified electrodes is calculated by using the following equation [38,39].

$$N_d = \frac{2}{e_0 \varepsilon \varepsilon_0} \Big/ \frac{d(1/C^2)}{dV}$$

where, the electron charge (e_0), relative permittivity (ε), and vacuum permittivity are 1.602 x 10^{-19} C, 48 and 8.854 x 10^{12} F m^{-1}, respectively. N_d and V are donor density and applied bias at the electrode. Fig. 5 (b, c, d, e) shows that the photocatalysts exhibit a positive slope in the Mott-Schottky plots indicating that they are n-type semiconductors. The N_d value was measured from the slope of Mott–Schottky plots and the flat band potential value was determined by extrapolation to a capacitance of zero. The calculated donor density and flat band potential (V_{Fb}) values of CdSNRs, CdSNRs/Ce_2S_3, NG-CdSNRs/$Ce_2S_3$are 7.610 x10^{13}, 1.3759 x 10^{16}, 2.020x10^{16} cm^{-3} and -0.89V, -1.02V, -1.11V, respectively. These results indicate that NG-CdSNRs/Ce_2S_3 photocatalyst has a higher donor density than the CdSNRs/Ce_2S_3 and CdSNRs. The higher donor density of NG-CdSNRs/Ce_2S_3, when combined with PL, TRPL, and impedance spectra suggest efficient charge carrier transfer than CdSNRs/$Ce_2S_3$and CdSNRs [40,41].

Generally, the conduction band (CB) edge potential of an n-type semiconductor is more negative (~0.10V) than the flat band potential [42,43]. Hence, the CB of CdSNRs, CdSNRs/Ce_2S_3 and NG-CdSNRs/Ce_2S_3 were calculate to be -0.791V, -0.920V and -1.011V *vs.* NHE, respectively. These potentials are more negative than the proton reduction potential (-0.41 V *vs.* NHE at pH = 7); therefore, NG-CdSNRs/Ce_2S_3 photocatalyst provides a much higher over-potential to reduce protons to produce H_2 from aqueous solution compared to CdSNRs/Ce_2S_3 and

CdSNRs. The E_{VB} values of CdSNRs, CdSNRs/Ce_2S_3, NG-CdSNRs/Ce_2S_3 were calculated to be 1.559V, 1.390V, 1.239V, respectively by following the equation $E_{CB}= E_{VB}- E_g$ [44]. These values are more positive than the redox potential of O_2/H_2O (0.82 V vs. NHE at pH = 7) [45–47].

To understand the charge transfer dynamics, a three-electrode electrochemical setup was used to measure photocurrent response. Figure 5 (f) shows the transient photocurrent responses of CdSNRs, CdSNRs/Ce_2S_3, and NG-CdSNRs/Ce_2S_3. The higher transient photocurrent response shown by NG-CdSNRs/Ce_2S_3 resulted from interface junction formation between CdSNRs and Ce_2S_3 and the high conductivity of N-doped graphene.

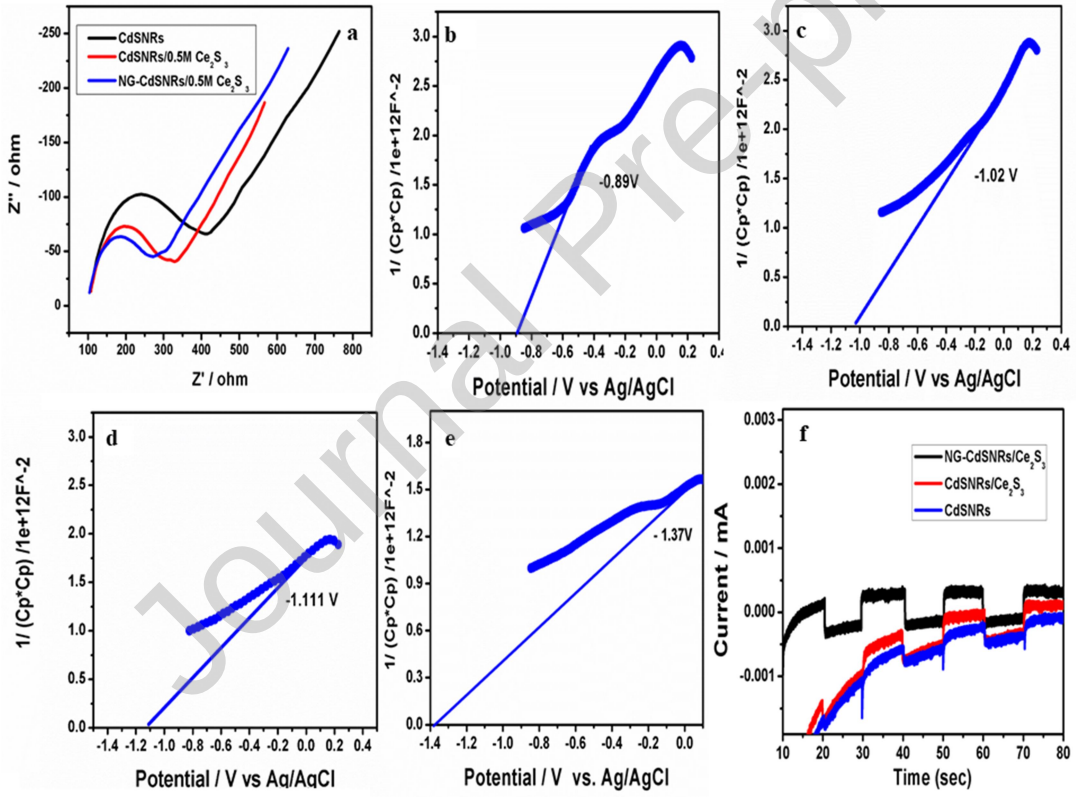

Figure 5 (a) Electrochemical impedance spectra of as-prepared CdSNRs, CdSNRs/ Ce_2S_3 and NG-CdSNRs/Ce_2S_3 photocatalysts; Mott-Schottky plots of (b) CdSNRs, (c) CdSNRs/Ce_2S_3, (d) NG-CdSNRs/Ce_2S_3 and (e) Ce_2S_3, and (f) photocurrent measurements of NG-CdSNRs/Ce_2S_3 photocatalysts

3.6. Solar light-driven H_2 production

The synthesized photocatalysts, CdSNRs, CdSNRs/Ce_2S_3, and NG-CdSNRs/Ce_2S_3were used for H_2 production reaction with Na_2S/Na_2SO_3 as a sacrificial reagent under natural solar light irradiation. Figure 6 (a) shows the photocatalytic activities of Ce_2S_3 coated on CdSNRs for H_2 production. The bare CdSNRs produced only 1498 μmol $h^{-1}g^{-1}$ of H_2 due to the rapid charge recombination rate [48] and the Ce_2S_3 generated a negligible amount of H_2. However, when CdSNRs were covered with 0.25M to 0.50M Ce_2S_3 nanoparticles, the hydrogen production rate also increased and reached a maximum of 16,181 μmol $h^{-1}g^{-1}$, which is ~ 10 times higher than the pure CdSNRs. The order of photocatalytic activity on different catalysts is CdSNRs/0.5MCe_2S_3 > CdSNRs/0.75MCe_2S_3 > CdSNRs/0.25MCe_2S_3 > CdSNRs/1.0MCe_2S_3 > CdSNRs/1.25MCe_2S_3 >CdSNRs > 0.5MCe_2S_3. As expected, the rate of H_2 production of CdSNRs/Ce_2S_3 is sharply enhanced due to the Ce_2S_3 coated on CdSNRs, indicating Ce_2S_3 performs very well as a co-catalyst [49–51].

Further increasing the amount of Ce_2S_3 in the catalyst from 0.50M (optimum level) to 1.25M, the rate of H_2 production (3189 μmol $h^{-1}g^{-1}$) decreased. Higher Ce_2S_3 amount in CdSNRs acts as a blocking layer for solar light absorption and leads to lower hydrogen production [52,53]. The higher hydrogen production shown by CdSNRs/Ce_2S_3 is in correlation with its improved visible light absorption and improved charge separation efficiency. To the best of our knowledge, this is the first report showing that Ce_2S_3 can be used as an efficient co-catalyst for H_2 production under solar light irradiation.

To further enhance the H_2 production rate, NG is incorporated into the CdSNRs/Ce_2S_3 photocatalysts as shown in Fig. 6(b). The results indicate that the amount of H_2 production is remarkably increasing with respect to increasing the amount of 1% NG (16,455 $\mu molh^{-1}g^{-1}$) to 3% NG (35,946 $\mu molh^{-1}g^{-1}$). The rate of production is almost double (from 16,181 to 35,946 $\mu mol\ h^{-1}g^{-1}$) when NG is incorporated with CdSNRs/Ce_2S_3. Hence, NG plays an important role in enriching the photocatalytic activity of NG-CdSNRs/Ce_2S_3. Further increasing the amount of NG (4wt%) leads to a reduced H_2 production rate (19,112 $\mu mol\ h^{-1}g^{-1}$), which is due to the excess amount of NG in the photocatalysts. This may increase the light scattering and also decrease the absorption of light by the photocatalyst [54,55]. These results are correlated to the UV-vis absorption spectra of different loading of NG in the nanocomposite [3% NG-CdSNRs/Ce_2S_3 given higher absorbance] (Fig. S4).

The excessive NG causes a shielding effect on the active sites present on the surface of photocatalysts and reduces the number of photo-generated electrons on the CdSNRs and photocatalytic reaction sites, respectively [56,57]. Here, 3% NG incorporated with CdSNRs/Ce_2S_3 is taken as an optimum level for the highest H_2 production (35946 $\mu mh^{-1}g^{-1}$), which is about 2 times higher than CdSNRs/0.5MCe_2S_3 (16181 $\mu molh^{-1}g^{-1}$) and ~24 times higher than bare CdSNRs, indicating that synergistic effect arises between the NG and CdSNRs/Ce_2S_3 photocatalysts.

The prepared photocatalyst has shown high H_2 production compared to the previously reported catalysts as compared in Table S1. The Solar to hydrogen (STH) efficiency of 1.29% was achieved with the as-prepared photocatalyst under solar light irradiation. These results indicate that the synthesized catalysts are efficient catalysts for solar light-driven H_2 production. This is further confirmed by a video taken during the H_2 production of the photocatalyst, a large

number of bubbles were frequently generated upon solar light irradiation in a glass cell filled with NG-CdSNRs/Ce_2S_3 photocatalyst. The enhancement of photocatalytic activities of NG-CdSNRs/$Ce_2S_3$is due to the presence of N atom doped graphene that increases the surface area of photocatalysts compared to CdSNRs/Ce_2S_3 and CdSNRs alone.

The stability of NG-CdSNRs/Ce_2S_3 photocatalysts was quantified with Na_2S/Na_2SO_3 sacrificial solution under simulated sunlight. The reaction system was evacuated to remove the evolved H_2 inside the glass reactor for every cycle. The same method was performed for 5 repeated cycles. There is negligible change in the reproduction of H_2 for NG-CdSNRs/Ce_2S_3 photocatalysts as shown in Fig. 6(c), indicating that prepared catalysts are more stable for H_2 production. TEM images and XRD data are also supporting that due to the coating of Ce_2S_3 cocatalyst on the CdSNRs, photo-corrosion of CdSNRs is retarded. Therefore, the hybrid NG-CdSNRs/Ce_2S_3 becomes highly stable.

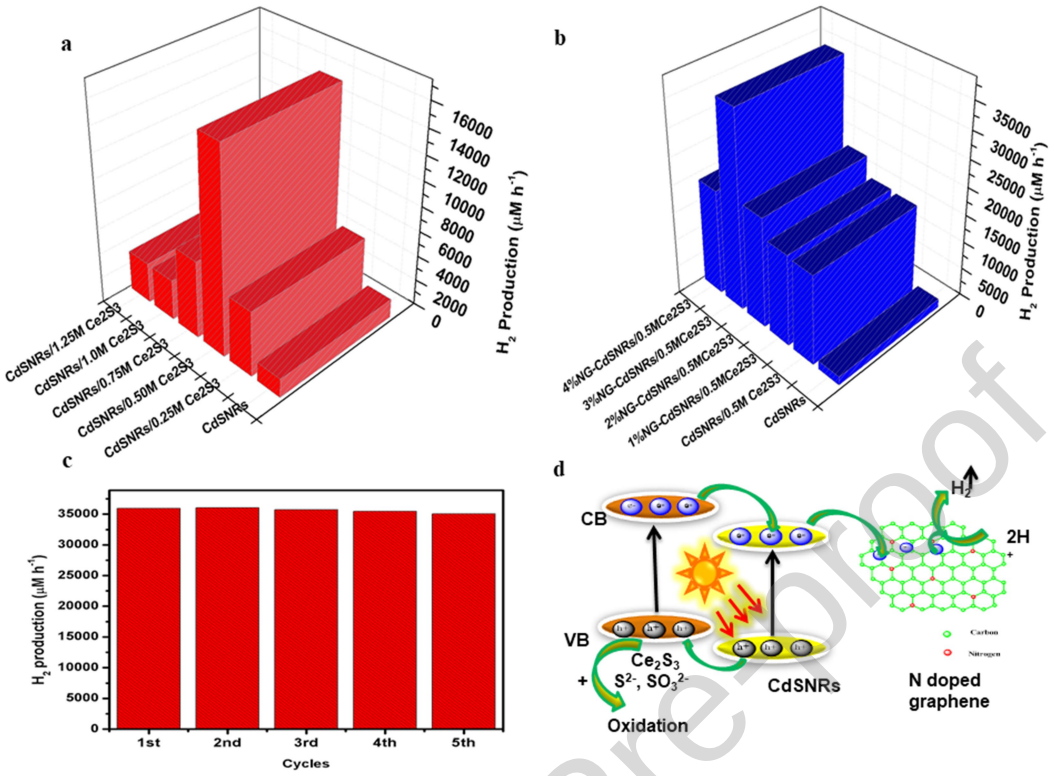

Figure. 6 Photocatalytic H_2 production rate of (a) CdSNRs/Ce_2S_3 (0.25, 0.50, 0.75, 1.00, 1.25M) samples, (b) CdSNRs, CdSNRs/0.5MCe_2S_3, 1, 2, 3 and 4% NG-CdSNRs/Ce_2S_3 samples under sunlight irradiation, (c) Reusability reaction of NG-CdSNRs/Ce_2S_3 sample under sunlight irradiation, and (d) the proposed photocatalytic H_2 production mechanism.

A proposed photocatalytic mechanism was proposed based on the obtained experimental data for photocatalytic H_2 production as given in Fig. 6(d). The CB potential of Ce_2S_3 samples is more negative (-1.271 V vs NHE) than the CB of pure CdSNRs (-0.791V vs NHE), So that, the transfer of the photo-induced electrons from Ce_2S_3 to CdSNRs is easily feasible at the interfaces. Additionally, photo-induced electrons are excited from VB to CB of CdSNRs during solar light irradiation. Hence, the numbers of photoelectrons are increased in the CB of CdSNRs, these CB

electrons in the CdSNRs have transferred via N-doped graphene (NG) in the catalysts. The NG is used as an electron conductor to improve the electron-hole pair separation and leave more charge carriers for effective H_2 production [58–61]. These photo-induced electrons are easily reduced by the protons present in the aqueous solution to produce H_2. At the same time, the transfers of photo-generated holes are trapped on the surface of Ce_2S_3 and lead to the anions (sulfide and sulfite ions) that induce the oxidation reaction.

3.7. Importance of sacrificial reagents

The main drawback of water splitting by a photocatalyst is that the process employing pure water is generally inefficient, and correlated to the oxidation and reduction reaction of water at the same time (in multistep reaction). The sacrificial reagents have been used as electron donors and holes scavenger for enhancing H_2 production [62]. In this work, S^{2-} ions and SO_3^{2-} ions can act as inorganic sacrificial reagents instead of alcohols because it is more easily oxidizable than the alcohols for H_2 production. It can accept holes and easily separate the electron-hole pair [63–65]. The usage of S^{2-} ions is an advantage for the production of H_2 using a CdS photocatalyst because the dissolved Cd^{2+} ions can interact with S^{2-} ions existing in the solution to reproduce the CdS catalyst. The general leaching of Cd^{2+} is largely prevented in this method. So that it retards the photo-corrosion of CdS and also stimulates the H_2 production through water-splitting reactions [66].

combination of S^{2-} and SO_3^{2-} ions containing solution is useful as a sacrificial agent for superior production of H_2 from the water. When sulfide (S^{2-}) ions are used alone for the production of H_2, they form disulfide (S_2^{2-}) ions, which have less negative reduction potential than the protons and also minimize the absorption of light by CdSNRs [67]. Therefore, SO_3^{2-} ions are an extra addition to the reaction solution and it interacts with disulfide ions to produce

sulfide ions. According to the previous reports [68], the following reaction mechanism was discussed in the production of H_2 using NG-CdSNRs/Ce_2S_3 photocatalyst in the presence of S^{2-} and SO_3^{2-} sacrificial agents. The photons were absorbed on the surface of CdSNRs to produce the electron-hole pairs under solar light irradiation (Equation-1) discussed as follows,

$h\nu > 420$ nm

$$CdSNRs + h\nu \longrightarrow h^+ + e^- \qquad \text{-----(1)}$$

Photogenerated electrons and holes were transferred to the surface of the photocatalyst and reacted with adsorbed water molecules or these electrons undergo recombination. Initially, the water molecule is reduced by the obtained electrons in the conduction band of the catalyst to produce H_2 (Equation-2). Simultaneously, oxidization of SO_3^{2-} ions and S_2^- ions to produce SO_4^{2-} and S_2^{2-} ions by the obtained holes in the valance band of the photocatalyst as described by Equations-3 and 4. Then, S_2^{2-} ions again interacted with SO_3^{2-} ions to produce $S_2O_3^{2-}$ and S^{2-} ions (Equation-5).

$$2e^- + 2H_2O \longrightarrow H_2 + 2OH^- \qquad \text{-------(2)}$$

$$SO_3^{2-} + 2OH^- + 2h^+ \longrightarrow SO_4^{2-} + 2H+ \qquad \text{-------(3)}$$

$$2S^{2-} + 2h^+ \longrightarrow S_2^{2-} \qquad \text{-------(4)}$$

$$S_2^{2-} + SO_3^{2-} \longrightarrow S_2O_3^{2-} + S^{2-} \qquad \text{-------(5)}$$

Additional S^{2-} ions present in the solution prevent the photo-corrosion of CdSNRs and also improve the efficiency of H_2 production. Moreover, $S_2O_3^{2-}$ ions do not interfere with protons in the reduction process.

4. Conclusion

In conclusion, we have synthesized Ce_2S_3 nanoparticles coated CdSNRs photocatalyst by the simple deposition-precipitation method and used it for a photocatalytic H_2 production application. When the coating of Ce_2S_3 on the surface of CdSNRs leads to the improved light absorption capacity of CdSNRs/Ce_2S_3 in the UV, Visible, and NIR regions. The photocatalytic production of H_2 was considerably increased in the presence of the Ce_2S_3 cocatalyst with the value of 16,181 μmol h^{-1} g^{-1} of H_2 under solar light irradiation, which is ~ 10 times higher than the pure CdSNRs. We have validated the N-doped graphene functionalized catalysts for considerable enhancement in photocatalytic H_2 production. At the optimal incorporation of N-doped graphene with CdSNR/Ce_2S_3, the H_2 production rate further enhanced is up to 35,946 μmol $h^{-1}g^{-1}$, which is 24 times higher than pure CdSNRs. (1) The absorption enhancement of the NG-CdSNRs/Ce_2S_3 photocatalyst in the visible region, (2) the efficient charge separation at the interface of CdSNRs and Ce_2S_3, and (3) the presence of NG in the catalyst could prevent the electron-hole pair recombination during the photocatalytic activity were confirmed by UV-vis, PL, TRPL, and impedance studies. These synergistic effects provide better photocatalytic activity of NG-CdSNRs/Ce_2S_3 for H_2 production. Similarly, NG-CdSNRs/Ce_2S_3 photocatalysts showed excellent stability up to 5 continuous cycles. The higher stability was achieved due to the covering of CdSNRs by NG and Ce_2S_3 nanoparticles, which effectively separated the electrons and holes. Moreover, this work provides a new method for improving the H_2 production rate of CdS-based photocatalysts under solar light irradiation."

Acknowledgments

Dr. A. Daniel Arul Raj, thanks to the Science & Engineering Research Board (SERB*),* New Delhi, India for providing National Postdoctoral Fellowship [*PDF/2016/001209]*. The authors also thank the Department of Science and Technology-Solar Energy Research Initiative (DST-SERI) [File No: DST/TM/SERI/S170(G)] for the financial support.

References:

[1] Y. Shi, X. Lei, L. Xia, Q. Wu, W. Yao, Enhanced photocatalytic hydrogen production activity of CdS coated with Zn-anchored carbon layer, Chemical Engineering Journal. 393 (2020) 124751. https://doi.org/10.1016/j.cej.2020.124751.

[2] (a)T. Hu, K. Dai, J. Zhang, S. Chen, Noble-metal-free Ni_2P modified step-scheme $SnNb_2O_6$/CdS-diethylenetriamine for photocatalytic hydrogen production under broadband light irradiation, Appl Catal B. 269 (2020) 118844. https://doi.org/10.1016/j.apcatb.2020.118844. (b)H.B. Gray, Powering the planet with solar fuel, Nat Chem. 1 (2009) 7–7. https://doi.org/10.1038/nchem.141. (c) M.S. Dresselhaus, I.L. Thomas, Alternative energy technologies, Nature. 414 (2001) 332–337. https://doi.org/10.1038/35104599.

[3] A.J. Bard, M.A. Fox, Artificial Photosynthesis: Solar Splitting of Water to Hydrogen and Oxygen, Acc Chem Res. 28 (1995) 141–145. https://doi.org/10.1021/ar00051a007.

[4] D.A. Reddy, E.H. Kim, M. Gopannagari, R. Ma, P. Bhavani, D.P. Kumar, T.K. Kim, Enhanced Photocatalytic Hydrogen Evolution by Integrating Dual Co-Catalysts on Heterophase CdS Nano-Junctions, ACS Sustain Chem Eng. 6 (2018) 12835–12844. https://doi.org/10.1021/acssuschemeng.8b02098.

[5] A. Fujishima, K. Honda, Electrochemical Photolysis of Water at a Semiconductor Electrode, Nature. 238 (1972) 37–38. https://doi.org/10.1038/238037a0.

[6] S.K. Lakhera, R.T. Pangal, H.Y. Hafeez, B. Neppolian, Oxygen-Functionalized and Ni^{+x} (x= 2, 3)-Coordinated Graphitic Carbon Nitride Nanosheets with Long-Life Deep-Trap

States and their Direct Solar-Light-Driven Hydrogen Evolution Activity, ChemSusChem. 12 (2019) 4293–4303. https://doi.org/10.1002/cssc.201901224.

[7] S.K. Lakhera, B. Neppolian, Role of molecular oxygen on the synthesis of $Ni(OH)_2/TiO_2$ photocatalysts and its effect on solar hydrogen production activity, Int J Hydrogen Energy. 45 (2020) 7627–7640. https://doi.org/10.1016/j.ijhydene.2019.10.142.

[8] A.R.M. Shaheer, V. Vinesh, S.K. Lakhera, B. Neppolian, Reduced graphene oxide as a solid-state mediator in $TiO_2/In_{0.5}WO_3$ S-scheme photocatalyst for hydrogen production, Solar Energy. 213 (2021) 260–270. https://doi.org/10.1016/j.solener.2020.11.030.

[9] A. Modak, K. Yamanaka, Y. Goto, S. Inagaki, Photocatalytic H_2 evolution by Pt-loaded 9,9'-Spirobifluorene-based conjugated microporous polymers under visible-light irradiation, Bull. Chem. Soc. Jpn. 89, (2016) 887–891. https://doi.org/ 10.1246/bcsj.20160105.

[10] A. Modak, K. Yamanaka, Y. Goto, S. Inagaki, Photocatalytic H_2 evolution by Pt-loaded 9,9'-Spirobifluorene-based conjugated microporous polymers under visible-light irradiation, Bull. Chem. Soc. Jpn. 89, (2016) 887–891. https://doi.org/ 10.1246/bcsj.20160105.

[11] G. Liu, C. Kolodziej, R. Jin, S. Qi, Y. Lou, J. Chen, D. Jiang, Y. Zhao, C. Burda, MoS_2 - Stratified CdS-$Cu_{2-x}S$ Core–Shell Nanorods for Highly Efficient Photocatalytic Hydrogen Production, ACS Nano. 14 (2020) 5468–5479. https://doi.org/10.1021/acsnano.9b09470.

[12] A. Kudo, Y. Miseki, Heterogeneous photocatalyst materials for water splitting, Chem. Soc. Rev. 38 (2009) 253–278. https://doi.org/10.1039/B800489G.

[13] J. Yang, D. Wang, H. Han, C. Li, Roles of Cocatalysts in Photocatalysis and Photoelectrocatalysis, Acc Chem Res. 46 (2013) 1900–1909. https://doi.org/10.1021/ar300227e.

[14] L. Dai, Y. Xue, L. Qu, H.-J. Choi, J.-B. Baek, Metal-Free Catalysts for Oxygen Reduction Reaction, Chem Rev. 115 (2015) 4823–4892. https://doi.org/10.1021/cr5003563.

[15] L. Jia, D.-H. Wang, Y.-X. Huang, A.-W. Xu, H.-Q. Yu, Highly Durable N-Doped Graphene/CdS Nanocomposites with Enhanced Photocatalytic Hydrogen Evolution from

Water under Visible Light Irradiation, The Journal of Physical Chemistry C. 115 (2011) 11466–11473. https://doi.org/10.1021/jp2023617.

[16] B. Mutharani, M. Keerthi, S.M. Chen, P. Ranganathan, T.W. Chen, S.Y. Lee, W.H. Chang, One-Pot Sustainable Synthesis of Ce_2S_3/Gum Arabic Carbon Flower Nanocomposites for the Detection of Insecticide Imidacloprid, ACS Appl. Mater. Interfaces 12 (2020) 4980–4988. https://doi.org/10.1021/acsami.9b16123.

[17] Y. Nakibli, Y. Mazal, Y. Dubi, M. Wächtler, L. Amirav, Size Matters: Cocatalyst Size Effect on Charge Transfer and Photocatalytic Activity, Nano Lett. 18 (2018) 357–364. https://doi.org/10.1021/acs.nanolett.7b04210.

[18] T. Wang, L.Yang, D. Jiang, H. Cao, A.C. Minja, P. Du, CdS Nanorods Anchored with Crystalline FeP Nanoparticles for Efficient Photocatalytic Formic Acid Dehydrogenation, ACS Appl. Mater. Interfaces 13 (2021) 23751–23759. https://doi.org/10.1021/acsami.1c04178.

[19] B. He, R. Liu, J. Ren, C. Tang, Y. Zhong, Y. Hu, One-Step Solvothermal Synthesis of Petalous Carbon-Coated Cu^{+}-Doped CdS Nanocomposites with Enhanced Photocatalytic Hydrogen Production, Langmuir. 33 (2017) 6719–6726. https://doi.org/10.1021/acs.langmuir.7b01450.

[20] H. Zhou, Q. Liu, W. Liu, J. Ge, M. Lan, C. Wang, J. Geng, P. Wang, Template-Free Preparation of Volvox-like $Cd_xZn_{1-x}S$ Nanospheres with Cubic Phase for Efficient Photocatalytic Hydrogen Production, Chem Asian J. 9 (2014) 811–818. https://doi.org/10.1002/asia.201301428.

[21] A.V. Murugan, T. Muraliganth, A. Manthiram, Rapid, Facile Microwave-Solvothermal Synthesis of Graphene Nanosheets and Their Polyaniline Nanocomposites for Energy Strorage, Chemistry of Materials. 21 (2009) 5004–5006. https://doi.org/10.1021/cm902413c.

[22] R. Mohan, A. Modak, A. NH_3-Plasma pre-treated carbon supported active iron–nitrogen catalyst for oxygen reduction in acid and alkaline electrolytes, Catal. Sci. Technol. 10, (2020) 1675–1687. https://doi.org/10.1039/C9CY0254F.

[23] Z. Tian, S. Dai, D. Jiang, Stability and Core-Level Signature of Nitrogen Dopants in Carbonaceous Materials, Chemistry of Materials. 27 (2015) 5775–5781. https://doi.org/10.1021/acs.chemmater.5b02370.

[24] Y.K. Kim, H. Park, Light-harvesting multi-walled carbon nanotubes and CdS hybrids: Application to photocatalytic hydrogen production from water, Energy Environ. Sci. 4 (2011) 685–694. https://doi.org/10.1039/C0EE00330A.

[25] M. Srivastava, A.K. Das, P. Khanra, Md.E. Uddin, N.H. Kim, J.H. Lee, Characterizations of in situ grown ceria nanoparticles on reduced graphene oxide as a catalyst for the electrooxidation of hydrazine, J Mater Chem A Mater. 1 (2013) 9792. https://doi.org/10.1039/c3ta11311f.

[26] S. Kumar, A.K. Ojha, D. Patrice, B.S. Yadav, A. Materny, One-step in situ synthesis of CeO_2 nanoparticles grown on reduced graphene oxide as an excellent fluorescent and photocatalyst material under sunlight irradiation, Physical Chemistry Chemical Physics. 18 (2016) 11157–11167. https://doi.org/10.1039/C5CP04457J.

[27] C. Mao, Y. Zhao, X. Qiu, J. Zhu, C. Burda, Synthesis, characterization and computational study of nitrogen-doped CeO_2 nanoparticles with visible-light activity, Physical Chemistry Chemical Physics. 10 (2008) 5633. https://doi.org/10.1039/b805915b.

[28] J. Chen, S. Shen, P. Wu, L. Guo, Nitrogen-doped CeO_x nanoparticles modified graphitic carbon nitride for enhanced photocatalytic hydrogen production, Green Chemistry. 17 (2015) 509–517. https://doi.org/10.1039/C4GC01683A.

[29] J. Chen, X.-J. Wu, L. Yin, B. Li, X. Hong, Z. Fan, B. Chen, C. Xue, H. Zhang, One-pot Synthesis of CdS Nanocrystals Hybridized with Single-Layer Transition-Metal Dichalcogenide Nanosheets for Efficient Photocatalytic Hydrogen Evolution, Angewandte Chemie International Edition. 54 (2015) 1210–1214. https://doi.org/10.1002/anie.201410172.

[30] W. Zhang, Y. Wang, Z. Wang, Z. Zhong, R. Xu, Highly efficient and noble metal-free NiS/CdS photocatalysts for H2 evolution from lactic acid sacrificial solution under visible light, Chemical Communications. 46 (2010) 7631. https://doi.org/10.1039/c0cc01562h.

[31] H. Rubin, D.J. Arent, B.D. Humphrey, A.B. Bocarsly, Overlayer Formation as a Source of Stability in the N-Type Photoelectrochemical Cell: The Cell, J Electrochem Soc. 134 (1987) 93–101. https://doi.org/10.1149/1.2100444.

[32] Jiang, Z. Sun, H. Jia, D. Lu, P. Du, A cocatalyst-free CdS nanorod/ZnS nanoparticle composite for high-performance visible-light-driven hydrogen production from water, J Mater Chem A Mater. 4 (2016) 675–683. https://doi.org/10.1039/C5TA07420G.

[33] S. Dutta, R. Sahoo, C. Ray, S. Sarkar, J. Jana, Y. Negishi, T. Pal, Biomolecule-mediated CdS-TiO_2 -reduced graphene oxide ternary nanocomposites for efficient visible light-driven photocatalysis, Dalton Transactions. 44 (2015) 193–201. https://doi.org/10.1039/C4DT02749C.

[34] T. Peng, K. Li, P. Zeng, Q. Zhang, X. Zhang, Enhanced Photocatalytic Hydrogen Production over Graphene Oxide–Cadmium Sulfide Nanocomposite under Visible Light Irradiation, The Journal of Physical Chemistry C. 116 (2012) 22720–22726. https://doi.org/10.1021/jp306947d.

[35] A. Modak, R. Mohan, K. Rajavelu, R. Cahan, T. Bendikov, A. Schechter, Metal−Organic Polymer-Derived Interconnected Fe−Ni Alloy by Carbon Nanotubes as an Advanced Design of Urea Oxidation Catalysts, ACS Appl. Mater. Interfaces 13 (2021) 8461−8473. https://dx.doi.org/10.1021/acsami.0c22148.

[36] A. D. Arulraj, M. Vijayan, J. Samseya, V. S. Vasantha, A Simple and Highly Sensitive Electrochemically Reduced p-Nitrobenzoic Acid Film Modified Sensor for Determination of Mercury, Electroanalysis 2014, 26, 2773 – 2782, http://dx.doi.org/10.1002/elan.201400460.

[37] L. Ye, J. Fu, Z. Xu, R. Yuan, Z. Li, Facile One-Pot Solvothermal Method to Synthesize Sheet-on-Sheet Reduced Graphene Oxide (RGO)/$ZnIn_2S_4$ Nanocomposites with Superior Photocatalytic Performance, ACS Appl Mater Interfaces. 6 (2014) 3483–3490. https://doi.org/10.1021/am5004415.

[38] C. Zhao, H. Luo, F. Chen, P. Zhang, L. Yi, K. You, A novel composite of TiO2 nanotubes with remarkably high efficiency for hydrogen production in solar-driven water splitting, Energy Environ Sci. 7 (2014) 1700. https://doi.org/10.1039/c3ee43165g.

[39] G. Wang, H. Wang, Y. Ling, Y. Tang, X. Yang, R.C. Fitzmorris, C. Wang, J.Z. Zhang, Y. Li, Hydrogen-Treated TiO_2 Nanowire Arrays for Photoelectrochemical Water Splitting, Nano Lett. 11 (2011) 3026–3033. https://doi.org/10.1021/nl201766h.

[40] Y. Zheng, Y. Jiao, L.H. Li, T. Xing, Y. Chen, M. Jaroniec, S.Z. Qiao, Toward Design of Synergistically Active Carbon-Based Catalysts for Electrocatalytic Hydrogen Evolution, ACS Nano. 8 (2014) 5290–5296. https://doi.org/10.1021/nn501434a.

[41] X. An, X. Yu, J.C. Yu, G. Zhang, CdS Nanorods/Reduced Graphene Oxide Nanocomposites for Photocatalysis And Electrochemical Sensing, J Mater Chem A Mater. 1 (2013) 5158. https://doi.org/10.1039/c3ta00029j.

[42] S. Saha, G. Das, J. Thote, R. Banerjee, Photocatalytic Metal–Organic Framework from CdS Quantum Dot Incubated Luminescent Metallohydrogel, J Am Chem Soc. 136 (2014) 14845–14851. https://doi.org/10.1021/ja509019k.

[43] Y.-J. Yuan, H.-W. Lu, Z.-T. Yu, Z.-G. Zou, Noble-Metal-Free Molybdenum Disulfide Cocatalyst for Photocatalytic Hydrogen Production, ChemSusChem. 8 (2015) 4113–4127. https://doi.org/10.1002/cssc.201501203.

[44] J. He, J. Wang, Y. Chen, J. Zhang, D. Duan, Y. Wang, Z. Yan, A dye-sensitized Pt@UiO-66(Zr) metal–organic framework for visible-light photocatalytic hydrogen production, Chem. Commun. 50 (2014) 7063–7066. https://doi.org/10.1039/C4CC01086H.

[45] X. Li, J. Yu, J. Low, Y. Fang, J. Xiao, X. Chen, Engineering heterogeneous semiconductors for solar water splitting, J Mater Chem A Mater. 3 (2015) 2485–2534. https://doi.org/10.1039/C4TA04461D.

[46] D.P. Kumar, S. Hong, D.A. Reddy, T.K. Kim, Noble metal-free ultrathin MoS_2 nanosheet-decorated CdS nanorods as an efficient photocatalyst for spectacular hydrogen evolution under solar light irradiation, J Mater Chem A Mater. 4 (2016) 18551–18558. https://doi.org/10.1039/C6TA08628D.

[47] J. Choi, D. Amaranatha Reddy, N.S. Han, S. Jeong, S. Hong, D. Praveen Kumar, J.K. Song, T.K. Kim, Modulation of charge carrier pathways in CdS nanospheres by integrating MoS_2 and Ni_2P for improved migration and separation toward enhanced photocatalytic hydrogen evolution, Catal Sci Technol. 7 (2017) 641–649. https://doi.org/10.1039/C6CY02145J.

[48] K. Wu, Y. Du, H. Tang, Z. Chen, T. Lian, Efficient Extraction of Trapped Holes from Colloidal CdS Nanorods, J Am Chem Soc. 137 (2015) 10224–10230. https://doi.org/10.1021/jacs.5b04564.

[49] K. Chang, Z. Mei, T. Wang, Q. Kang, S. Ouyang, J. Ye, MoS_2 /Graphene Cocatalyst for Efficient Photocatalytic H_2 Evolution under Visible Light Irradiation, ACS Nano. 8 (2014) 7078–7087. https://doi.org/10.1021/nn5019945.

[50] K. Zhang, W. Kim, M. Ma, X. Shi, J.H. Park, Tuning the charge transfer route by p–n junction catalysts embedded with CdS nanorods for simultaneous efficient hydrogen and oxygen evolution, J Mater Chem A Mater. 3 (2015) 4803–4810. https://doi.org/10.1039/C4TA05571C.

[51] T. Jia, A. Kolpin, C. Ma, R.C.-T. Chan, W.-M. Kwok, S.C.E. Tsang, A graphene dispersed CdS–MoS_2 nanocrystal ensemble for cooperative photocatalytic hydrogen production from water, Chem. Commun. 50 (2014) 1185–1188. https://doi.org/10.1039/C3CC47301E.

[52] Q. Li, B. Guo, J. Yu, J. Ran, B. Zhang, H. Yan, J.R. Gong, Highly Efficient Visible-Light-Driven Photocatalytic Hydrogen Production of CdS-Cluster-Decorated Graphene Nanosheets, J Am Chem Soc. 133 (2011) 10878–10884. https://doi.org/10.1021/ja2025454.

[53] J. Yu, T. Ma, S. Liu, Enhanced photocatalytic activity of mesoporous TiO_2 aggregates by embedding carbon nanotubes as electron-transfer channel, Phys. Chem. Chem. Phys. 13 (2011) 3491–3501. https://doi.org/10.1039/C0CP01139H.

[54] X.-Y. Zhang, H.-P. Li, X.-L. Cui, Y. Lin, Graphene/TiO_2 nanocomposites: synthesis, characterization and application in hydrogen evolution from water photocatalytic splitting, J Mater Chem. 20 (2010) 2801. https://doi.org/10.1039/b917240h.

[55] L. Jia, D.-H. Wang, Y.-X. Huang, A.-W. Xu, H.-Q. Yu, Highly Durable N-Doped Graphene/CdS Nanocomposites with Enhanced Photocatalytic Hydrogen Evolution from Water under Visible Light Irradiation, The Journal of Physical Chemistry C. 115 (2011) 11466–11473. https://doi.org/10.1021/jp2023617.

[56] J. Zhang, J. Yu, M. Jaroniec, J.R. Gong, Noble Metal-Free Reduced Graphene Oxide-$Zn_x Cd_{1-x} S$ Nanocomposite with Enhanced Solar Photocatalytic H_2 -Production Performance, Nano Lett. 12 (2012) 4584–4589. https://doi.org/10.1021/nl301831h.

[57] Q. Xiang, J. Yu, M. Jaroniec, Enhanced photocatalytic H2-production activity of graphene-modified titania nanosheets, Nanoscale. 3 (2011) 3670. https://doi.org/10.1039/c1nr10610d.

[58] R. Czerw, B. Foley, D. Tekleab, A. Rubio, P.M. Ajayan, D.L. Carroll, Substrate-interface interactions between carbon nanotubes and the supporting substrate, Phys Rev B. 66 (2002) 033408. https://doi.org/10.1103/PhysRevB.66.033408.

[59] C.X. Guo, H.B. Yang, Z.M. Sheng, Z.S. Lu, Q.L. Song, C.M. Li, Layered Graphene/Quantum Dots for Photovoltaic Devices, Angewandte Chemie International Edition. 49 (2010) 3014–3017. https://doi.org/10.1002/anie.200906291.

[60] J. Hou, C. Yang, H. Cheng, Z. Wang, S. Jiao, H. Zhu, Ternary 3D architectures of CdS QDs/graphene/$ZnIn_2S_4$ heterostructures for efficient photocatalytic H_2 production, Physical Chemistry Chemical Physics. 15 (2013) 15660. https://doi.org/10.1039/c3cp51857d.

[61] A.P. Bhirud, S.D. Sathaye, R.P. Waichal, J.D. Ambekar, C.-J. Park, B.B. Kale, In-situ preparation of N-TiO_2 /graphene nanocomposite and its enhanced photocatalytic hydrogen production by H_2S splitting under solar light, Nanoscale. 7 (2015) 5023–5034. https://doi.org/10.1039/C4NR06435F.

[62] . Rechavi, D. Givol, E. Canaani, Activation of a cellular oncogene by DNA rearrangement: possible involvement of an IS-like element, Nature. 300 (1982) 607–611. https://doi.org/10.1038/300607a0.

[63] S. Saadi, A. Bouguelia, A. Derbal, M. Trari, Hydrogen photoproduction over new catalyst CuLaO2, J Photochem Photobiol A Chem. 187 (2007) 97–104. https://doi.org/10.1016/j.jphotochem.2006.09.017.

[64] T. Peng, K. Li, P. Zeng, Q. Zhang, X. Zhang, Enhanced Photocatalytic Hydrogen Production over Graphene Oxide–Cadmium Sulfide Nanocomposite under Visible Light Irradiation, The Journal of Physical Chemistry C. 116 (2012) 22720–22726. https://doi.org/10.1021/jp306947d.

[65] A. Boudjemaa, R. Bouarab, S. Saadi, A. Bouguelia, M. Trari, Photoelectrochemical H_2-generation over Spinel $FeCr_2O_4$ in X_2^- solutions, Appl Energy. 86 (2009) 1080–1086. https://doi.org/10.1016/j.apenergy.2008.06.007.

[66] J.F. Reber, M. Rusek, Photochemical hydrogen production with platinized suspensions of cadmium sulfide and cadmium zinc sulfide modified by silver sulfide, J Phys Chem. 90 (1986) 824–834. https://doi.org/10.1021/j100277a024.

[67] N. Buehler, K. Meier, J.F. Reber, Photochemical hydrogen production with cadmium sulfide suspensions, J Phys Chem. 88 (1984) 3261–3268. https://doi.org/10.1021/j150659a025.

[68] Tsuji, H. Kato, H. Kobayashi, A. Kudo, Photocatalytic H_2 Evolution Reaction from Aqueous Solutions over Band Structure-Controlled $(AgIn)_x Zn_{2(1-x)} S_2$ Solid Solution Photocatalysts with Visible-Light Response and Their Surface Nanostructures, J Am Chem Soc. 126 (2004) 13406–13413. https://doi.org/10.1021/ja048296m.

AUTHOR CONTRIBUTION STATEMENT

Daniel Arulraj Abraham: Conceptualization, Methodology, Validation, Investigation, Data Curation, Visualization, Formal analysis, Writing – original draft

Aswathy Rajan: Investigation, Formal analysis, Writing – Review & Editing

M. D. Dhileepan: Investigation, Formal analysis, Editing

Masakazu Anpo: Validation, Formal analysis, Writing - Review & Editing

Neppolian. B: Supervision, writing – review and editing, funding acquisition, resources

Declaration of interests

☒ The authors declare that they have no known competing financial interests or personal relationships that could have appeared to influence the work reported in this paper.

☐The authors declare the following financial interests/personal relationships which may be considered as potential competing interests:

Graphical Abstract

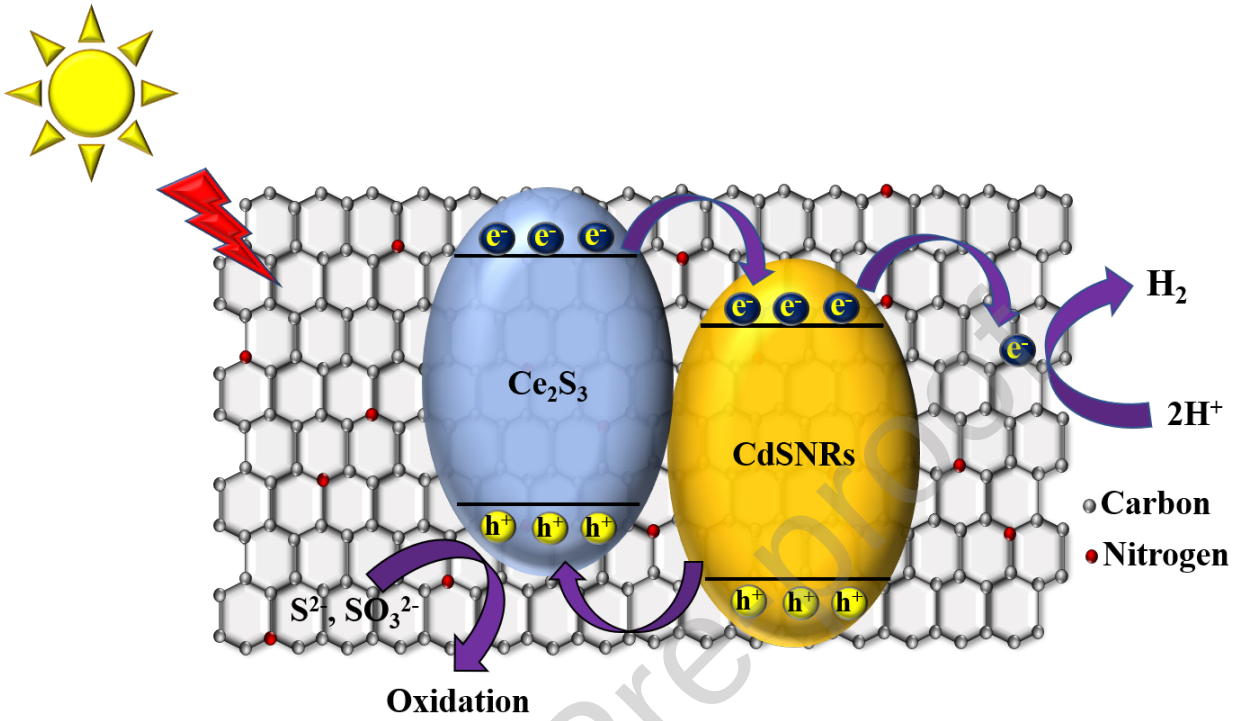

Highlights

- The NG-CdSNRs/Ce_2S_3 photocatalyst was prepared by a hydrothermal route.
- The CdS is deposited and coated uniformly over Ce_2S_3 and NG.
- NG-CdSNRs/Ce_2S_3 produced photocatalytic H_2 production rate of 35,946 μmol $h^{-1}g^{-1}$.
- H_2 production rate of NG-CdSNRs/Ce_2S_3 catalyst is 24 times higher than pristine